



Cite this: *Chem. Commun.*, 2021, **57**, 2372

Received 26th October 2020,
 Accepted 26th January 2021

DOI: 10.1039/d0cc07085h

rsc.li/chemcomm

Thermochromism and piezochromism of an atomically precise high-nuclearity silver sulfide nanocluster†

Qiao-Qiao Sun,^a Qian Li,^b Hai-Yang Li,^{*a} Miao-Miao Zhang,^a Meng-En Sun,^a Si Li,^a Zewei Quan^{ib} and Shuang-Quan Zang^{ib}

A novel high-nuclearity silver sulfide nanocluster [Ag₅₀S₇(SC₆H₄F)₃₆(dppp)₆]-4DMI, (hereafter abbreviated as 1-4DMI) was synthesised. Solvent-free crystals of **1 displayed a completely reversible narrowing and broadening of the optical band gap that was accompanied by visual thermochromism and piezochromism changeovers, when stimulated by varying temperatures between 113 and 413 K or by changing the pressure from 1 atm to 7.5 GPa.**

Silver sulfide Ag₂S has been intensively studied as the most in-demand semiconductor, which has potential application in optoelectronics, biosensors and catalysis.^{1–3} Among them, nanosized metal clusters have gained wide research interest since their well-defined structures, attractive size distribution and inherent properties can be applied in various areas, such as chemical sensing, biolabeling, drug delivery and medical therapy.^{1–3} In previous studies, significant progress has been made in the chemical synthesis and well-defined structural characterization of high-nuclear silver sulfide nanoclusters protected by thiolate or co-protected by thiolate and phosphine ligands.^{4–10} However, for most silver sulfide nanoclusters, their inherent instability, especially thermal instability, has hampered their potential application. To date, only a few low-nuclearity silver sulfide nanoclusters can resist high temperatures in air,^{11–13} and no high-nuclearity case has been reported.

Thermochromism is a phenomenon in which the luminescence or color of materials changes as the temperature increases or decreases.¹⁴ Thermochromic materials have been applied in a

variety of fields, including chemical anticounterfeiting, optical sensors, thermal energy storage materials, and smart windows.¹⁵ Many silver sulfide nanocluster crystals display thermochromic luminescence in a range of cryogenic and room temperatures.¹⁶ However, thermally induced color change and energy-gap modulation in a high-temperature range have not been reported. In addition, piezochromism is a new type of force response of intelligent materials that depicts luminescence or color variation under the application of pressure.^{17,18} Because the applied pressure appears as an independent thermodynamic parameter that can both compress and distort the structure of materials, pressure-induced optical color-changing materials have attracted wide attention in crystalline materials including halide perovskites and metal-organic frameworks.^{19,20} To date, only a few research studies have been conducted on the bulk crystals of atomically precise metal-cluster at high pressure.²¹

Herein, we prepared single crystals of a novel high-nuclearity silver sulfide nanocluster (**1-4DMI**) *via* a reaction between a silver-SC₆H₄F precursor and dppp in a mixture of DMI and trichloromethane at room temperature, (DMI = 1,3-dimethyl-2-imidazolidinone, dppp = 1,3-bis(diphenylphosphino)propane). Solvent-free crystals of [Ag₅₀S₇(SC₆H₄F)₃₆(dppp)₆] (**1**) demonstrate unusual thermal stability in air up to 413 K. When the crystals of **1** were subjected to continuously varying temperatures between 113 and 413 K and varying hydrostatic pressures between 1 atm and 7.5 GPa in a diamond anvil cell (DAC), continuously reversing thermochromism and piezochromism was observed. Temperature-dependent powder X-ray diffraction (PXRD) and pressure-dependent Raman spectra demonstrated that no obvious phase transformation occurred during the thermochromism and piezochromism processes. This work shows that temperature and pressure can significantly tailor the electronic structure of metal clusters, resulting in the potential discovery of novel physical phenomena and new cluster materials under high pressure.

Single-crystal structural analysis revealed that **1-4DMI** crystallized in the monoclinic space group *P*2₁/*c*. Cluster **1** was

^a Green Catalysis Center and College of Chemistry, Zhengzhou University, Zhengzhou 450001, China. E-mail: lihaiyang@zzu.edu.cn

^b Department of Chemistry, Academy for Advanced Interdisciplinary Studies, Shenzhen Engineering Research Center for Frontier Materials Synthesis at High Pressures, Southern University of Science and Technology (SUSTech), Shenzhen, Guangdong 518055, China. E-mail: quanzw@sustech.edu.cn

† Electronic supplementary information (ESI) available: Experimental details, powder X-ray diffraction, thermal analysis, and additional figures. CCDC 1992657–1992659. For ESI and crystallographic data in CIF or other electronic format see DOI: 10.1039/d0cc07085h

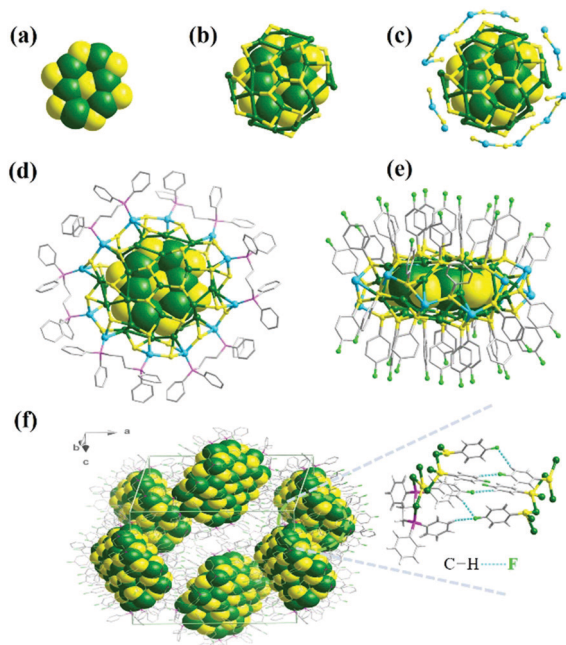


Fig. 1 (a) Ag_6S_7 core in the space-filling mode. (b) Ag_6S_7 encapsulated in the $\text{Ag}_{32}\text{S}_{22}$ shell in the stick mode. (c) $\text{Ag}_6\text{S}_7@Ag_{32}S_{22}$ surrounded by the $\text{Ag}_{12}\text{S}_{14}$ motif around the waist. (d) Top view of $\text{Ag}_6\text{S}_7@Ag_{32}S_{22}@Ag_{12}S_{14}$ protected by dppp ligands. (e) Side view of $\text{Ag}_6\text{S}_7@Ag_{32}S_{22}@Ag_{12}S_{14}$ by the $-\text{SC}_6\text{H}_4\text{F}$ ligand. (f) Stacking of the $[\text{Ag}_{50}\text{S}_7(\text{SC}_6\text{H}_4\text{F})_{36}(\text{dppp})_6]$ cluster in a unit cell. Color code: green, Ag in the core and shell; turquoise, Ag in the waist; yellow, S; bright green, F; purple, P; gray, C.

comprised of 50 silver(I) ions bridged by 36- $\text{SC}_6\text{H}_4\text{F}$ ligands and seven S^{2-} ions together with six dppp ligands (Fig. S1, ESI[†]); structurally, Cluster 1 can be depicted as an Ag_6S_7 core encapsulated in an $\text{Ag}_{32}\text{S}_{22}$ shell (Fig. 1a and b). The $\text{Ag}_6\text{S}_7@Ag_{32}S_{22}$ core-shell structure is further surrounded by an $\text{Ag}_{12}\text{S}_{14}$ motif around the waist (Fig. 1c and d). The Ag_6S_7 core is composed of six Ag^+ and seven S^{2-} ions. From the coordination modes of S^{2-} ions, one of the seven S^{2-} ions is in the center and adopts a μ_4 -bridging mode that is coordinated to Ag^+ ions; the remaining S^{2-} ions function as μ_5 - and μ_6 -bridges binding both the core and $\text{Ag}_{32}\text{S}_{22}$ -shell Ag atoms (Fig. S2, ESI[†]). Each P atom of dppp ligands coordinates to one Ag atom. The bond lengths including Ag–Ag, Ag–S and Ag–P are listed in Table S1 (ESI[†]).

The $-\text{SC}_6\text{H}_4\text{F}$ groups which are located at the top and bottom of the disc-like clusters, point upward and downward (Fig. 1e). The weak intercluster $\text{C}-\text{H}\cdots\text{F}$ bonding and van der Waals interactions consolidate the stacking of the cluster in all three dimensions. A 2-fold screw axis appears along the $[0,1,0]$ direction at $1/4$, y , $1/4$, and the glide plane is perpendicular to the b axis with a glide component of $[1/2, 0, 1/2]$. Thus, two cluster 1 molecules are located on the surface of the (001) planes, and four clusters pass through the c axis in the unit cell (Fig. 1f). The phase purity of **1-4DMI** was confirmed by PXRD (Fig. S3, ESI[†]). The thermogravimetry (TG) curve shows a weight loss that occurs below 413 K, which corresponds to the 4 DMI molecules (Fig. S4, ESI[†]).

The thermal stability observed in the TG experiments encouraged us to examine the structural stability when the

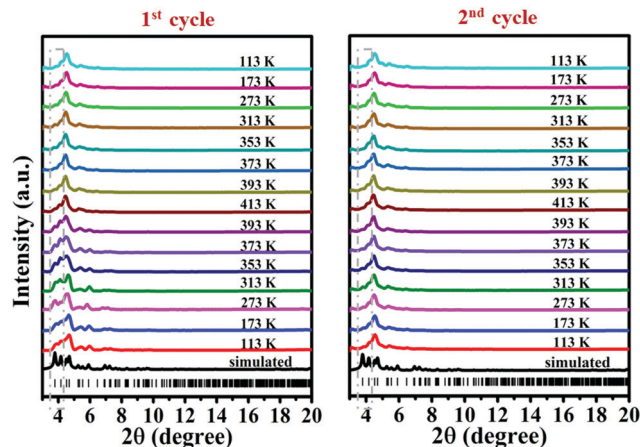


Fig. 2 *In situ* variable-temperature PXRD of **1-4DMI** during both heating and cooling cycles.

temperature was changed using temperature-dependent PXRD (Fig. 2). In the first cycle, the structure of **1-4DMI** nearly did not change between 113 K and 393 K since the diffraction patterns remain invariable. However, when the temperature increases from 393 K to 413 K, the diffraction peaks below a 2θ of 5° gradually disappear, suggesting the loss of the DMI solvent molecules, which corresponds to the TG results. During the cooling process when the temperature decreases from 413 K to 113 K, the diffraction patterns no longer change until the second cycle of temperature variation was finished. Such high thermal stability is very rare in atomically-precise silver sulfide nanoclusters.^{11–13}

Subsequently, we collected the crystal data of **1-4DMI** at 100 K, 150 K and 200 K (Table S2, ESI[†]). **1-4DMI** exhibits a phenomenon of volume expansion in the unchanged space group in the tested temperature range (Fig. S5 and Table S3, ESI[†]). Notably, at 200 K, the DMI molecules become disordered, and cannot be solved; at 298 K, many of the silver atoms become even more disordered. Thus, we could not obtain useful crystallographic data of solvent-free **1**. Instead, we plotted the function of the unit-cell parameters *versus* temperature in a temperature range of 100–260 K (Fig. S6, ESI[†]), which suggested that thermal expansion should occur along the three axes of solvent-free **1**; furthermore, the unit-cell volume should expand, and thus the crystal size should increase (Fig. S7 and Table S4, S5, ESI[†]).

Interestingly, a synchronous temperature-dependent color change in the solvent-free crystals of **1** from yellow to dark red is observed from 113 to 413 K (Fig. 3a). The reversibility of the color change is demonstrated by imaging for at least four heating and cooling cycles (Fig. 3b). UV-vis absorption spectra from 113–413 K varies in the range of 525–565 nm (Fig. 3c). Correspondingly, Tauc plots of the UV-vis spectra indicate that the band gap and temperature change are negatively correlated, and the former decreases from 2.28 to 2.10 eV with increasing temperature (Fig. 3e). The large band gap may be caused by the quantum confinement effect as the dimensions of the Ag_{50} cluster is close to the exciton Bohr radius of about 2 nm for

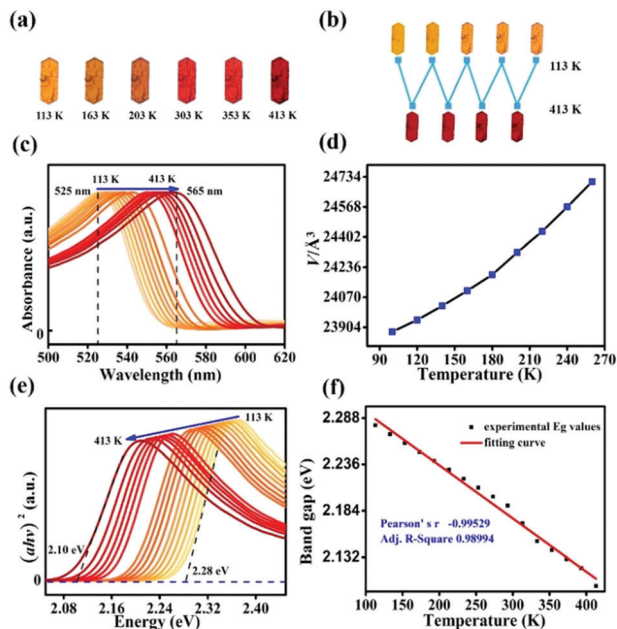


Fig. 3 (a) Alternating colors in a single crystal of **1** from 113 to 413 K. (b) Varying colors of **1** in a four-cycle test. (c) Temperature-dependent solid state UV-vis absorption spectra and (e) the corresponding Tauc plots recorded from 113 to 413 K. (d) Unit-cell volume of **1** versus temperature. (f) Plots displaying the linear relationship between the band gap and temperature.

Ag_2S .²² The relationship between the band gap and temperature presents an approximately linear relationship that can be described by the following equation, $E_g = 2.354 - (5.956 \times 10^{-4}) \times T$ (Fig. 3f). Since no phase transformation occurs, and the transitions of the thiolated silver(i) clusters generally originate from metal-to-ligand charge-transfer (MLCT) that are modified by Ag–Ag interactions,²³ the synchronous expansion of crystals and the increase in orbital hybrids may be induced by the increase in the degree of disorder of the metal atoms. The above observations may collectively induce a decrease in the energy gap of the crystals as the temperature increases (Fig. 3d). The negative temperature effects are characteristic of typical semiconductors, and they tend to decrease with increasing temperature.²⁴

The bond length and volume-dependent energy gap during the thermochromic phenomenon further inspired us to investigate the pressure response of this cluster crystal, which is a newly developed research field in atomically-precise metal clusters. Subsequently, the pressure-dependent optical spectra of **1** were measured using a DAC. The extraordinary piezochromic transition of **1** is seen in the optical micrographs. Upon compression, the original orange-red gradually changes to translucent dark red at 7.5 GPa, and the color reverses after decompression (Fig. 4a). The reversible color change phenomenon can be maintained for at least two cycles (Fig. S8, ESI†). Correspondingly, the absorption spectra also return to the initial state (Fig. S9 and S10, ESI†). Selected UV-vis absorption spectra of **1** upon compression are depicted in Fig. 4b. Under ambient conditions, the absorption edge is observed at approximately 586 nm, and the absorption edge gradually redshifts to 670 nm at 7.5 GPa.

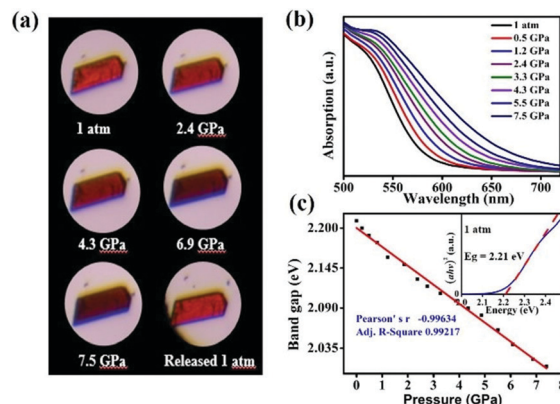


Fig. 4 (a) Optical micrographs of **1** in a DAC upon compression. (b) Selected high-pressure absorption spectra of **1** from ambient conditions to 7.5 GPa. (c) Direct band gap evolution of **1** as a function of pressure, as calculated from Tauc plots. The inset shows the band gap Tauc plots at 1 atm, and the red line represents the linearly fitted curve.

The evolution of the optical band gap can be effectively evaluated according to the movement of the absorption edge. Thus, Tauc plots are implemented to determine the band gap variations. Fig. 4c depicts the relationship between the direct band gap and pressure, which presents an approximately linear relationship that can be described by the following equation, $E_g = 2.200 - (2.609 \times 10^{-2}) \times P$. The band gap of **1** undergoes a continuously noticeable decrease from ambient conditions to 7.5 GPa, indicating a negative correlation between the band gap and pressure. In addition, the functional relationship between the indirect band gap and pressure shows a similar trend (Fig. S11, ESI†). Thus, the band gap transition regardless of its direct or indirect nature is modulated by a pressure-induced shrinkage of bond,²⁵ thus, an increase in pressure can promote the overlapping of elemental orbitals.²⁵ In addition, the decreases in the band gap induced by high temperature and high pressure seem to be contradictory. We tentatively propose that high temperature may cause an increase in both atomic distances and electron sharing owing to a weakened binding force, and the latter is probably the dominant source of the gap narrowing. In addition, the number of atoms in the unit cell is too large to calculate the details for this type of semiconductor, which will be overcome in the future.

The pressure-dependent Raman spectra of **1** were recorded to investigate the possibility of a structural change. At ambient pressure, the Raman spectra consist of ten strong vibrational modes with a frequency distribution from 50 cm^{-1} to 1200 cm^{-1} (Fig. S12 and S13, ESI†).²⁶ With increasing pressure, most vibrational modes show normal blueshifts, which may be attributed to the reduction in the interatomic distance. The blueshift of the lattice vibration of ν_1 is the fastest among all vibrational modes²⁷ (Fig. S14, ESI†), suggesting the shrinkage of Ag–Ag bonds. The vibrational modes are no longer observed when the pressure reaches 4.6 GPa, probably because of masking that is induced by a high fluorescence background. Pressure-induced fluorescence background is commonly observed in a variety of materials, especially organic materials.²⁸ Such fluorescence background is too weak to be clearly observed in photoluminescence

spectra. However, it can influence the detection of Raman signals. In our materials, it is inferred that the organic ligands could induce a fluorescence background at high pressure, limiting the further Raman detection of inorganic clusters. The vibrational modes are restored after decompression, indicating deformation reversibility. The second cycle of compression–decompression still shows complete reversibility of the crystal structure. The small reduction in ν_1 and the ν_4 mode upon decompression can be attributed to pressure-induced defects and the local disorder of the crystal. Therefore, there is no observation of phase transition in the Raman experiments, and the crystal structure is reversible after decompression.

In summary, we have successfully prepared and characterized a novel high-nuclearity silver sulfide nanocluster that features a multilayer core–shell structure and unusual stability at a high temperature in air. The temperature and pressure can modulate the optical band gap of the cluster crystals, leading to reversible thermochromism and piezochromism in the visible light range that is unprecedented among metal clusters. This work broadens the application of noble metal nanoclusters as temperature or pressure probes and represents a breakthrough in the field of metal nanoclusters.

We acknowledge the support for this work from the National Science Fund for Distinguished Young Scholars (21825106), the National Natural Science Foundation of China (No. 21671175 and 21801227), the Program for Innovative Research Team (in Science and Technology) in Universities of Henan Province (19IRTSTHN022), Zhengzhou University and the Shenzhen Engineering Research Center for Frontier Materials Synthesis at High Pressures.

Conflicts of interest

There are no conflicts to declare.

Notes and references

- (a) J. N. Anker, W. P. Hall, O. Lyandres, S. J. Zhao and R. P. Duyne, *Nat. Mater.*, 2008, **7**, 442–453; (b) R.-W. Huang, Y.-S. Wei, X.-Y. Dong, X.-H. Wu, C.-X. Du, S.-Q. Zang and T. C. W. Mak, *Nat. Chem.*, 2017, **9**, 689–697; (c) I. Chakraborty and T. Pradeep, *Chem. Rev.*, 2017, **117**, 8208–8271; (d) S. I. Sadovnikov, A. A. Rempel and A. I. Gusev, *Russ. Chem. Rev.*, 2018, **87**, 303–327; (e) S. I. Sadovnikov, A. I. Gusev and A. A. Rempel, *Rev. Adv. Mater. Sci.*, 2015, **41**, 7–19.
- (a) Y. Tao, M. Li, J. Ren and X. Qu, *Chem. Soc. Rev.*, 2015, **44**, 8636–8663; (b) S. I. Sadovnikov, A. I. Gusev and A. A. Rempel, *Superlattices Microstruct.*, 2015, **83**, 35–47; (c) S. I. Sadovnikov, A. I. Gusev and A. A. Rempel, *Phys. Chem. Chem. Phys.*, 2015, **17**, 12466–12471; (d) A. I. Gusev, S. I. Sadovnikov, A. V. Chukin and A. A. Rempel, *Phys. Solid State*, 2016, **58**, 251–257.
- (a) X.-R. Song, N. Goswami, H.-H. Yang and J. Xie, *Analyst*, 2016, **141**, 3126–3140; (b) S. I. Sadovnikov, A. A. Rempel and A. I. Gusev, *Russ. Chem. Rev.*, 2018, **87**, 303–327; (c) S. I. Sadovnikov and A. I. Gusev, *Eur. J. Inorg. Chem.*, 2016, 4944–4957; (d) S. I. Sadovnikov and A. I. Gusev, *J. Mater. Chem. A*, 2017, **5**, 17676–17704.
- H. Yang, Y. Wang, H. Huang, L. Gell, L. Lehtovaara, S. Malola, H. Häkkinen and N. Zheng, *Nat. Commun.*, 2013, **4**, 2422–2425.
- W. Du, S. Jin, L. Xiong, M. Chen, J. Zhang, X. Zou, Y. Pei, S. Wang and M. Zhu, *J. Am. Chem. Soc.*, 2017, **139**, 1618–1624.
- S. Jin, S. Wang, Y. Song, M. Zhou, J. Zhong, J. Zhang, A. Xia, Y. Pei, M. Chen, P. Li and M. Zhu, *J. Am. Chem. Soc.*, 2014, **136**, 15559–15565.
- M. J. Alhilaly, M. S. Bootharaju, C. P. Joshi, T. M. Besong, A.-H. Emwas, R. Juárez-Mosqueda, S. Kaappa, S. Malola, K. Adil, A. Shkurenko, H. Hakkinen, M. Eddaoudi and O. M. Bakr, *J. Am. Chem. Soc.*, 2016, **138**, 14727–14732.
- S. Bestgen, O. Fuhr, B. Breitung, V. S. K. Chakravadhanula, G. Guthausen, F. Hennrich, W. Yu, M. M. Kappes, P. W. Roesky and D. Fenske, *Chem. Sci.*, 2017, **8**, 2235–2240.
- I. Chakraborty, A. Govindarajan, J. Erusappan, A. Ghosh, T. Pradeep, B. Yoon, R. L. Whetten and U. Landman, *Nano Lett.*, 2012, **12**, 5861–5866.
- C. E. Anson, A. Eichhofer, I. Issac, D. Fenske, O. Fuhr, P. Sevillano, C. Persau, D. Stalke and J. Zhang, *Angew. Chem., Int. Ed.*, 2008, **47**, 1326–1331.
- S. Li, Z.-Y. Wang, G.-G. Gao, B. Li, P. Luo, Y.-J. Kong, H. Liu and S.-Q. Zang, *Angew. Chem., Int. Ed.*, 2018, **57**, 12775–12779.
- Z.-Y. Wang, M.-Q. Wang, Y.-L. Li, P. Luo, T.-T. Jia, R.-W. Huang, S.-Q. Zang and T. C. W. Mak, *J. Am. Chem. Soc.*, 2018, **140**, 1069–1076.
- Z. Han, X.-Y. Dong, P. Luo, S. Li, Z.-Y. Wang, S.-Q. Zang and T. C. W. Mak, *Sci. Adv.*, 2020, **6**, eaay0107.
- (a) K. Miyata, Y. Konno, T. Nakanishi, A. Kobayashi, M. Kato, K. Fushimi and Y. Hasegawa, *Angew. Chem., Int. Ed.*, 2013, **52**, 6413–6416; (b) B. Sun, X.-F. Liu, X.-Y. Li, Y. Cao, Z. Yan, L. Fu, N. Tang, Q. Wang, X. Shao, D. Yang and H.-L. Zhang, *Angew. Chem., Int. Ed.*, 2020, **59**, 203–208.
- (a) J. Lin, M. Lai, L. Dou, C. S. Kley, H. Chen, F. Peng, J. Sun, D. Lu, S. A. Hawks, C. Xie, F. Cui, A. P. Alivisatos, D. T. Limmer and P. Yang, *Nat. Mater.*, 2018, **17**, 261–267; (b) S. Kumar, A. Qadir, F. Maury and N. Bahlawane, *ACS Appl. Mater. Interfaces*, 2017, **9**, 21447–21456.
- Z. Wang, J.-W. Liu, H.-F. Su, Q.-Q. Zhao, M. Kurmoo, X.-P. Wang, C.-H. Tung, D. Sun and L.-S. Zheng, *J. Am. Chem. Soc.*, 2019, **141**, 17884–17890.
- S. Liu, S. Sun, C. K. Gan, A. G. Águila, Y. Fang, J. Xing, T. T. H. Do, T. J. White, H. Huang, W. Li and Q. Xiong, *Sci. Adv.*, 2019, **5**, eaav9445.
- (a) Q. Li, L. Yin, Z. Chen, K. Deng, S. Luo, B. Zou, Z. Wang, J. Tang and Z. Quan, *Inorg. Chem.*, 2019, **58**, 1621–1626; (b) Z.-Q. Yao, J. Xu, B. Zou, Z. Hu, K. Wang, Y.-J. Yuan, Y.-P. Chen, R. Feng, J.-B. Xiong, J. Hao and X.-H. Bu, *Angew. Chem., Int. Ed.*, 2019, **58**, 5614–5618; (c) S. Jiang, Y. Fang, R. Li, H. Xiao, J. Crowley, C. Wang, T. White, W. Goddard III, Z. Wang, T. Baikie and J. Fang, *Angew. Chem., Int. Ed.*, 2016, **55**, 6540–6544.
- Y. Shi, Z. Ma, D. Zhao, Y. Chen, Y. Cao, K. Wang, G. Xiao and B. Zou, *J. Am. Chem. Soc.*, 2019, **141**, 6504–6508.
- (a) W.-Q. Liao, J.-D. Zhao, Y.-Y. Tang, Y. Zhang, P.-F. Li, P.-P. Shi, X.-G. Chen, Y.-M. You and R.-G. Xiong, *Science*, 2019, **363**, 1206–1210; (b) Q. Qi, J. Qian, X. Tan, J. Zhang, L. Wang, B. Xu, B. Zou and W. Tian, *Adv. Funct. Mater.*, 2015, **25**, 4005–4010.
- Q. Li, M. A. Mosquera, L. O. Jones, A. Parakh, J. Chai, R. Jin, G. C. Schatz and X. W. Gu, *ACS Nano*, 2020, **14**, 11888–11896.
- (a) Z.-Y. Chen, D. Y. S. Tam and T. C. W. Mak, *Chem. Commun.*, 2016, **52**, 6119–6122; (b) X. He, Y. Wang, C.-Y. Gao, H. Jiang and L. Zhao, *Chem. Sci.*, 2015, **6**, 654–658.
- V. W.-W. Yam, K. K.-W. Lo, W. K.-M. Fung and C.-R. Wang, *Coord. Chem. Rev.*, 1998, **171**, 17–41.
- K.-Y. Wang, D. Ding, S. Zhang, Y.-L. Wang, W. Liu, S.-A. Wang, S.-H. Wang, D. Liu and C. Wang, *Chem. Commun.*, 2018, **54**, 4806–4809.
- Q. Li, Y. Wang, W. Pan, W. Yang, B. Zou, J. Tang and Z. Quan, *Angew. Chem., Int. Ed.*, 2017, **56**, 15969–15973.
- A. Jolivet, R. Fablet, J.-F. Bardeau and H. D. Pontual, *Anal. Bioanal. Chem.*, 2013, **405**, 4787–4798.
- L. Zhang, C. Liu, L. Wang, C. Liu, K. Wang and B. Zou, *Angew. Chem., Int. Ed.*, 2018, **57**, 11213–11217.
- Q. Li, S. Li, K. Wang, W. Li, J. Liu, B. Liu, G. Zou and B. Zou, *J. Chem. Phys.*, 2012, **137**, 184905.